Journal of Molecular Structure 1273 (2023) 134279

Contents lists available at ScienceDirect

Journal of Molecular Structure

journal homepage: www.elsevier.com/locate/molstr

Copper(I) iodide complex with 4-pyridinecarboxaldehyde ligand: Synthesis, spectroscopic characterisation, AIM and NCI analysis combined with molecular docking and antibacterial activity studies

Sibel Celik[a,*], Senay Yurdakul[b], Belgin Erdem[a]

[a] Department of Health Care Services, Kırşehir Ahi Evran University, Kırşehir, Turkey
[b] Department of Physics, Faculty of Science, Gazi University, Ankara, Turkey

ARTICLE INFO

Article history:
Received 16 July 2022
Revised 15 September 2022
Accepted 3 October 2022
Available online 4 October 2022

Keywords:
DFT
Copper complex
Pyridinecarboxaldehyde
Molecular docking
Antibacterial activity

ABSTRACT

In this article, we synthesized a [CuI(4-pyridinecarboxaldehyde)$_4$] complex characterized by CHN analyses, FT-IR, UV-Vis, and DFT. The spectroscopic characteristics and biological activities of the synthesized complex were investigated using quantum mechanical methods using combined experimental and computational approaches. The orbital NBO and topological AIM approaches were used to investigate intermolecular interactions. According to the second-order perturbation energy analysis, the majority of the $E^{(2)}$ stabilization energies of of LP(N) → LP*(Cu) are higher than those of LP(I) → LP*(Cu), implying that the nitrogen atom in the complex is the main contributor to coordination. In addition, the biological activities of the title complex were investigated by using molecular docking analysis. In this investigation, the title Cu (I) complex was the most active molecule, with the maximum antibacterial activity against *S. aureus* and *S. epidermidis* infections that should be further clinically investigated due to its effective anti and anti-quorum sensing properties. The title complex showed good antiquorum-sensing activity when tested against *C. violaceum* ATCC 12472. Furthermore, in-silico molecular docking investigations corroborated the chemical activity correlations. The Cu (I) combination has a maximum dock score for some of the active chemicals.

1. Introduction

Copper complexes have been recognized as potential antibacterial, anticancer, and antioxidant chemicals due to their advantageous redox properties and are regarded as one of the most promising anticancer agents, second only to cisplatin [1–5]. Antimalarial, antifungal, Alzheimer's illness, Parkinson's disease, amyotrophic lateral sclerosis, diabetes, inflammatory conditions (i.e. rheumatoid arthritis), skin wounds, cardiovascular diseases, and leishmaniasis are all treated using copper complexes [6]. Furthermore, Cu(I) complexes are extremely important in the discovery of metal-based drugs from transition metal complexes. Because copper is an endogenous metal with high coordination ability and low toxicity compared to exogenous metals (ruthenium, iridium, and platinum. etc.) [5]. There is significant evidence that copper complexes may represent successful alternatives to clinically accepted platinum-based drugs [7]. The fact that many tumor cells, including breast and prostate cancer cells, use more copper than normal cells suggests that copper is strongly associated with tumor cells. Such as ceruloplasmine and superoxide dismutase, which perform fundamental biological tasks vital to cellular growth and development [8]. Schiff base copper complexes have been shown in the literature to inhibit certain cancer cell development *in vitro* and in human tumor cell cultures [9,10]. Copper is a structural and catalytic cofactor of various enzymes [7], with variable oxidation states of Cu(II) and Cu(I) that act as anti-tumor agents, and a back and forth shift between these two oxidation states via single electron transfer reactions. Copper's biological involvement is primarily in redox processes and as a biological catalyst [11–13].

Nitrogen heterocycles, in particular pyridine molecules bearing carbonyl groups, known as gem-diols, are commonly utilized in catalysis, environmental chemistry, medicine, hydrometallurgy, and biotechnology [14]. Additionally, metal complexes of N-donor ligands have demonstrated extraordinary antibacterial activity against bacteria and fungi [15]. 4-Pyridinecarboxaldehyde is a heterocyclic building block that can be used to make many different pharmaceuticals, like new 1,4-dihydropyridin-4-yl-phenoxyacetohydrazones that have anticonvulsant and anti-inflammatory properties [16,17]. The Korich-type reaction uses 4-pyridinecarboxaldehyde as a building block for the production of

* Corresponding author.
E-mail address: sibelcelik@ahievran.edu.tr (S. Celik).

https://doi.org/10.1016/j.molstruc.2022.134279
0022-2860/

Schiff bases. Metal complexes of several of these Schiff bases have been demonstrated to have strong antibacterial and antifungal action, as well as modest nuclease activity [18]. Schiff base Cu(II) and Co(II)-pyridinecarboxaldehyde complexes have previously been studied [14] using NMR, single crystal X-ray diffraction, and EPR in conjunction with theoretical DFT calculations. In this paper, we describe the synthesis and characterization of the 4-pyridinecarboxaldehyde (4-Py-CHO) ligand with a copper(I) ion. The Cu(I)-4-pyridinecarboxaldehyde complex was studied using FT-IR and UV-Vis spectroscopy, as well as elemental analysis. Additionally, DFT calculations of this compound were performed and compared with the experimental data. Non-covalent interactions are important in pharmaceutical design, supramolecular chemistry, molecular biology, and other chemical disciplines [19]. Therefore, we performed non-covalent interactions (NCIs) and AIM and NBO analyzes to explain these interactions, which include hydrogen bonding, π-π stacking, cation-π, electrostatic, hydrophobic and Van der Waals forces. The molecular docking method is used to describe a molecule's interaction with a protein at the atomic level, which permits categorizing tiny molecules' behavior at the binding sites of target proteins and so elucidating their essential biochemical processes [20]. This approach may predict the ligand-protein binding affinity as well as the structure of protein-ligand complexes. It is a crucial tool in structural molecular biology and computer-aided drug design. Finding active compounds from existing chemicals is typically the initial stage in the development of novel drugs [21]. Our research aims to evaluate the antibacterial activity of the Cu (I) complex against clinically significant bacterial pathogens as well as the effectiveness of the complex's antiquorum sensing capability. The antibacterial and antiquorum-sensing activities of the Cu(I) complex were investigated to support and compare the molecular docking results.

2. Experimental

2.1. Synthesis of complex

Sigma-Aldrich purchased copper iodide and 4-pyridinecar boxaldehyde, which were utilized without purification. In 20 mL of ethanol, the ligand (4-Py-CHO) (2 mmol; 214.22 mg) was liquefied. Then, with steady mixing at 50 °C, CuI (1 mmol; 190.45 mg) was progressively added to the first produced solution. 3 h of constant stirring at the same temperature To allow the solvent to evaporate, the finished solution was stored at room temperature for one week. The metal-to-ligand ratio in the produced compound is 1:4. Under ambient conditions, the colorless metal complex was filtered and dried. The complexation was performed in a 100 mL glass vessel equipped with a mechanical stirrer. The synthesized chemical has a 76% yield. The following calculated and experimental values for CHN analyses were reported: [CuI($C_6H_5NO)_4$], [CuI$C_{24}H_{20}N_4O_4$], CHN Calc: C: 46.58%, H: 3.30%, N: 9.05%, Found: C: 47.80%, H: 3.90%, N: 8.86%.

2.2. Instrumentation for recording spectra

On the Bruker Vertex 80 FT-IR spectrometer, the [CuI(4-Py-CHO)$_4$] complex's infrared spectra was acquired between 4000 and 550 cm^{-1}. The Far-IR spectra were obtained on the Bruker IFS 66/S system between 700 and 100 cm^{-1}. An Agilent HP 8453 spectrophotometer was used to record the UV–Vis spectrum in a quartz cell using DMSO as the solvent. Thermogravimetric analysis (TGA) was performed in a dynamic N_2 atmosphere (40 mL/min) with a heating rate of 25 °C/min from a surrounding temperature of 1000 °C/min using a Mettler Toledo thermal analyzer.

2.3. Antibacterial and antiquorum-sensing properties

Ten different bacterial cultures were used (*S.aureus* ATCC 29213, *S.epidermidis* ATCC 35984, *L. monocytogenes* ATCC 35152, *B. subtilis* ATCC 6633, *B. cereus* 709 Roma, *E. faecalis* ATCC 29212, *E. coli* ATCC 25922, *S. typhimurium* ATCC 14028, *P. aeruginosa* ATCC 27853 and *K. pneumoniae* ATCC 13883). Bacteria used in the study were obtained from the Culture Collection of Kırşehir Ahi Evran University, Department of Biology.

The antibacterial activity of substances was determined in this experiment using the *minimal inhibitor concentration (MIC)* and the agar well diffusion method. The NCCLS guidelines were used to determine the minimum inhibitory concentrations (MIC) of compounds against bacteria [22].

In the bacterial suspension (0.5 McFarland), test solutions (1000 μg/ml in DMSO), and MIC tests, Mueller-Hinton broth (Oxoid) was utilized. The test microorganisms were inoculated into Nutrient Broth (Difco) and incubated at 37 °C for 24-48 h.

Bacteria were grown in agar well diffusion for 24–48 h (10^5 bacteria per mL). Culture plate wells were pierced with a sterile cork borer drill (7 mm in diameter) and filled with a dissolved compound containing 10% DMSO (10 mg/mL). The inhibition zones (mm) on the agar plates were then measured in millimeters. The positive control was ampicillin (AMP) (10 μg), and the negative control was dimethylsulfoxide (DMSO). For each step of the disk diffusion method, the NCCLS guidelines were followed [23].

The test was performed three times, and the findings are shown as a mean. The obtained agar well diffusion zone sizes were compared to the conventional antibiotic ampicillin.

The antipathogenic potential of the compound was determined by antiquorum sensing activity against *C. violaceum* ATCC 12472 in LB agar (Luria Bertani) medium. A culture of *C. violaceum* (1×10^6) was spread on the LB agar surface. Next, wells were drilled in LB agar with a cork borer and the tested chemical (5 mg/mL) was added to the wells.

The plates were incubated at 30 °C for 24 h to measure the suppression of pigment production around the well. The good results included stopping the growth of bacteria and making a clear halo around the disc.

3. Computational details

In this study, DFT/B3LYP/GEN level theory with the Gaussian09 program [24], DGDZVP basis set for Cu, I atoms, and 6–311G++(d,p) basis set for all the non-metal atoms were used. Harmonic vibrational frequencies computed were often greater than measured values. As a result, the calculated wavenumbers were scaled using 0.967 scaling factors [25]. The complete theoretical vibrational distribution analysis of the Cu(I) iodide complex was procured based on TED (Total Energy Distribution) analysis with the same level of theory that has been done with the PQS (Parallel Quantum Solutions) software [26]. The electronic properties of MEP and FMO's visualization of the achieved results were obtained by the GaussView software [27]. The Natural Bond Orbital (NBO) analysis has been done by using the NBO 5.0 [19] program, which is integrated into the Gaussian 09W package. The computed UV–Vis spectra were estimated using the TD-DFT/CAM-B3LYP approach with the DGDZVP basis set, and the solvent action was properly considered using the IEFPCM model. Multiwfn [28] and molecular visualization program VMD [29] were used to determine the intensity of non-covalent interactions (NCIs), the isodensity surface plot, and the reduced density gradient (RDG) surface. Moreover, partial density of states (PDOS) are generated with multiwfn software. Auto dock 4.2.6 Tools were used to construct the initial structures to run the docking simulations. The world's largest online protein database, RCSB, is the major source

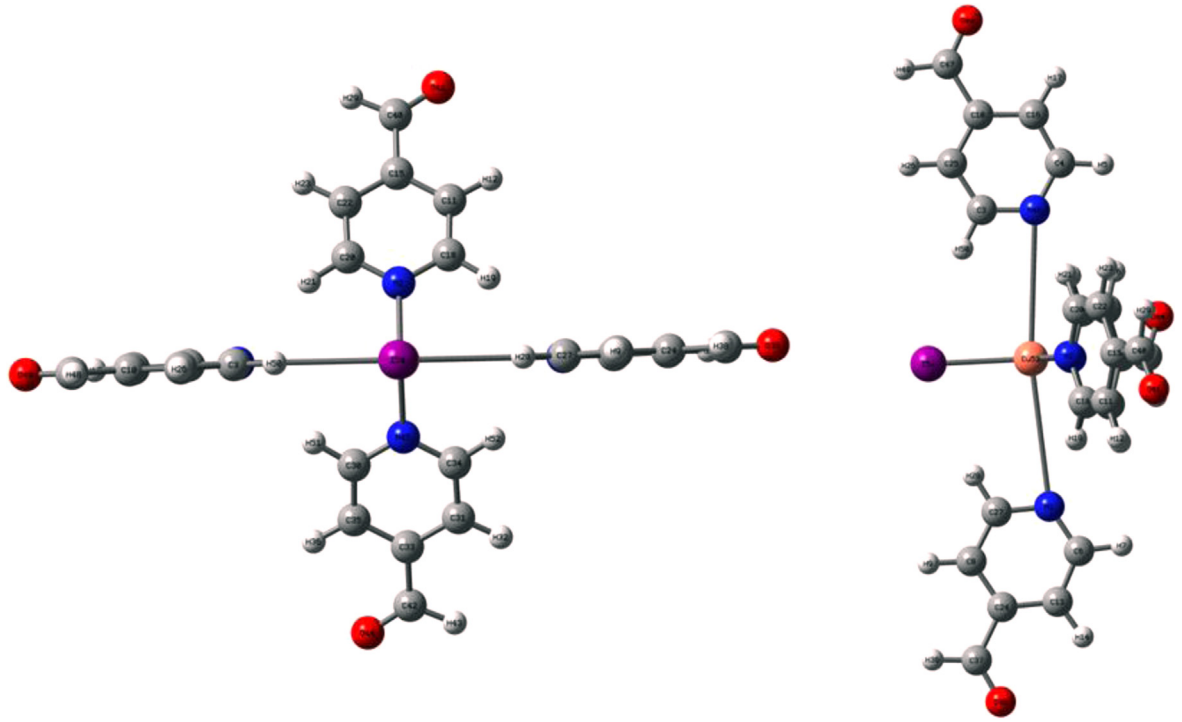

Fig. 1. Optimized geometric structure with atom numbering of the Cu(I) complex.

for collecting the PDB structures used as target proteins. The gram –ve bacteria (*Staphylococcus epidermidis*, PDB ID: 3KP3). the receptor of gram +ve bacteria (*Staphylococcus aureus*, PDB ID: 1JIJ), ⟨13:italic ⟩Chromobacterium violaceum⟨/13:italic⟩ (PDB ID: 3QP1) was obtained from the RCSB Protein Data Bank (www.pdb.org). The docked poses were visualized using the PyMOL software [30] and Chimera [31].

4. Results and discussion

4.1. Description of the optimized structure

Geometrical parameters are extremely important in theoretical studies of organic compounds since they are used to determine the molecule's stability. The transition metal complexes of the ligands containing N,O-donor sites have unusual configurations and structural liabilities [19]. In this article, we synthesized a Cu(I) complex that can be accounted for by the N atoms of the ligand's pyridine ring when combined with metal and the presence of an iodide ion within the field of coordination. The [CuI(4-Py-CHO)$_4$] complex (Fig. 1) was optimized for geometry. In particular, the X-ray structure of the title complex is still not yet established experimentally. So, the starting structure of this complex is described in the literature [14] M(I)-3-pyridinecarboxaldehyde and M(I)-4-pyridinecarboxaldehyde (M=Cu or Co) in the same square planar copper to four pyridine coordination. The geometry of the copper complex synthesized by Kargar et al. [32] was taken into account when the iodine atom was linked to the metal ion in our study. It is taken from the structure that suggests it is coordinated by the nitrogen in pyridine rings and the iodine atom. Observations have been made on the geometric parameters of the metal complex mentioned in Table 1 that indicate the mode of bonding between ligand donor atoms and the metal ion. The ligand forms a 4:1 complex with copper and iodine through coordination through nitrogen atoms to form a stable geometry around the central metal ion. The coordination sphere is formed by N atoms occupying the ligands' equatorial positions, while the coordinating iodide occupies the axial site. This coordination has been observed in similar structures found in previous research [32]. The optimization results showed that the title compound is coordinated with the ligand N-donor groups. As shown in Fig. 1, the protons of the two groups rotate and diverge. According to the optimized structure, the 4-Py-CHO ligands are coordinated to the metal core through the pyridine nitrogen atoms. The Cu–N1, Cu–N45 bond distances are 2.026 Å. These Cu-N bond distances are in good agreement with those reported in other similar copper complexes [32–34]. Furthermore, the average Cu-I bond length is 2.6317(4) Å, which is comparable to other copper iodide coordination polymers, such as 2.7147(7) Å for [CuI(6-Me-quinoline)]n [35], 2.587(3) Å for [{Cu(μ3-I)}2(4.2′- pypzpy)2{Cu(μ-I)}2]n [36], 2.869 Å and 2.6633(7) Å for [Cu2I2(Apyz)]n [37]. From Table 1, the Cu–I distance is 2.586 Å, which is compatible with the literature and shows the participation of the Cu(I) ion has coordination geometry with the I^- ion. The Cu−I bond distance and N−Cu−I angles are within the range of reported values for such copper iodide compounds.

4.2. Vibrational spectroscopy

DFT calculations were used to calculate the vibrational frequencies of the synthesized compound. The vibration analysis of the Cu(I) iodide complex was carried out on the basis of the characteristic vibrations present in the complex. Theoretical and experimental vibrational wavenumbers are given in Table S1 comparatively. The calculated vibrational frequencies were multiplied by a scaling factor of 0.967 to obtain corrected values closer to the experimental data. The experimental FT-IR spectra of the free ligand and its copper(I) iodide complex, recorded in the range of 4000–400 cm^{-1} are given in Fig. 2, and the Far-IR spectra of the complex is given in Fig. S1.

The experimental and computational vibration frequencies compared in table S1 show that the DFT and experimental results are in good agreement. The bands seen at 3260 and 3055 cm^{-1} (pyridine ring) and 2989 and 2903 cm^{-1} (aldehyde group) in the

Table 1
The DFT method was used to calculate selected bond lengths (Å) and angles (°) of the Cu(I) complex.

Bond Length		***Bond Length***		***Bond Length***	
Cu-N1	3.746	Cu-N45	2.026	Cu-I	2.586
Cu-N2	2.026	Cu-N46	3.744		
Bond Angle		***Bond Angle***		***Bond Angle***	
N1-Cu-N2	88.317	N2-Cu-N46	87.440	N2-Cu-I	119.214
N1-Cu-N45	87.443	N45-Cu-N46	88.376	N1-Cu-I	94.289
N2-Cu-N45	121.546	N45-Cu-I	119.238	N46-Cu-I	94.340

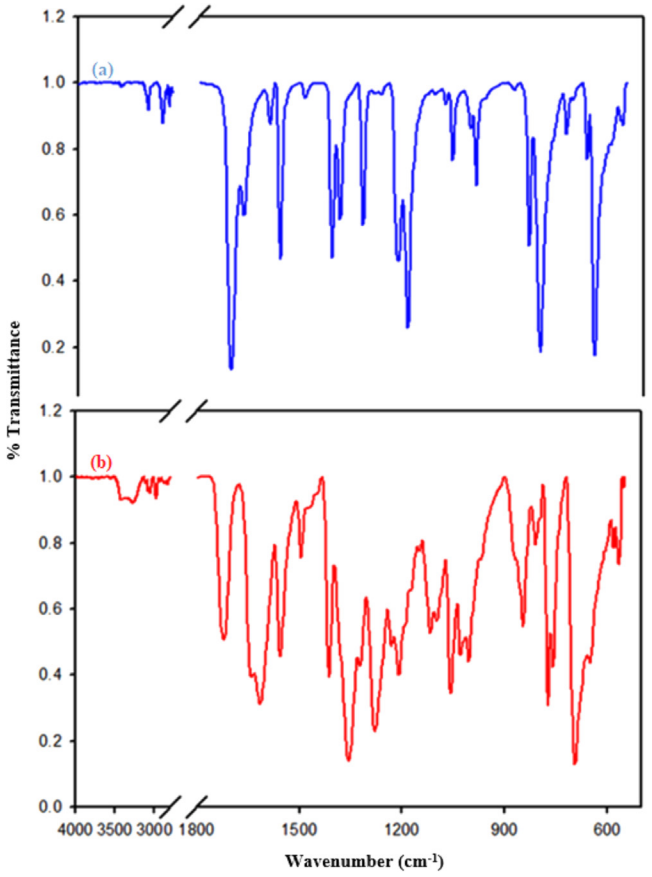

Fig. 2. Experimental FT-IR spectra of 4-Py-CHO ligand (a) and Cu(I) complex (b).

IR spectrum are attributed to C-H stretching vibration in the Cu(I) complex. In the IR spectrum, the C-C stretching pyridine ring vibrations appear at 1600-1450 cm^{-1} [38–40]. The C-C stretching mode appears as strong bands in the FT-IR spectrum at 1610 and at 1550 cm^{-1}. The theoretical values calculated for the C-H and C-C bands can be shown to be in accordance with the experimental results as well as those reported in the literature. The IR band assignments are useful in evaluating the coordination behavior of ligands with copper(I) ions. The C=O stretching vibrations, which are expected to be observed in the 1730–1700 cm^{-1} region according to the literature, were observed in the present study at 1710 cm^{-1} and 1708 cm^{-1} for the experimental and theoretical values for the Cu(I) complex, respectively. In the free ligand spectrum, the peaks corresponding to C=O stretching are observed at 1708 cm^{-1} (very strong). When the free ligand and the copper complex of the υ(C=O) stretching vibration of carbonyl group are compared, it is seen that there is no shift in this frequency value after complexation. These data suggest that the carboxyl group is not involved in the formation of the copper complex. This means that the carbonyl oxygen atoms are non-coordinated with the metal ion. On the other hand, the spectrum of ligand showed the characteristic ring stretching frequency υ(C=N) band at 1595 and 1560 cm^{-1} which was shifted to frequencies at 1610 and 1550 cm^{-1}, respectively. The υ(C-N) band of ligand was appeared at 1387, 1231, 1209, and 1004 cm^{-1}, which is shifted to lower frequencies in the spectra of the complexes at 1352, 1217, 1190 and 995 cm^{-1} for complex, respectively, with shifts due to coordination indicative of pyridine N atoms coordination to Cu(I) metal ion. The observed low energy shift of the band in the complex could be due to the decrease in the C=N double bond character, which suggests the coordination of the ligands to copper atoms [41,42].

Metal-ligand stretching and ring-deformation bands can be seen in the Far-IR spectrum. From the literature study, it is observed that the metal-nitrogen (M-N) and metal-iodine (M-I) stretching wavenumbers are exhibited in the lower frequency range [43,44]. The Far-IR spectrum of the Cu(I) complex showed the appearance of few additional bands not found in the spectra of the 4-Py-CHO ligand in the 600-50 cm^{-1} region, and this is the Cu-N and Cu-I [45,46]. In the present investigation, we have observed that the new bands at the medium bands (564 and 406 cm^{-1}) are attributed to υ(Cu-N) stretching. The bands observed at 111 and 137 cm^{-1} are ascribed to υ(Cu-I) stretching vibrations between Cu(I) and iodine atoms. In the table S1, DFT calculations with a sustained PED distribution are used to represent the remaining in-plane bending and the out-of-plane vibrations δ(CNCu), δ(NCuN), and δ(NCuI) of title complex. The results of the far-infrared spectroscopy were utilized to demonstrate the successful coordination of the ligand with copper and iodine. These vibrations are very similar to those reported in the literature by previous researchers for copper(I) iodide complexes [47–50].

4.3. UV–visible absorption spectra and TD/DFT calculations

As predicted by the TD-DFT/CAM-B3LYP/DGDZVP calculation in DMSO, the observed displacement points to a metallic center that is rich in electrons after the complex forms. This makes it harder to reduce the metal because of the interactions between the species [51]. The most effective theoretical approach to luciberate the dynamic and static characteristics of molecules in an excited state is the TD-DFT method [45]. Table 2 shows experimental and theoretical absorption wavelengths, band gaps, oscillator strength (f), excitation energy, and major contributions to electronic transitions, whereas Fig. 3 shows experimental UV-visible absorbance and transmittance spectra. The longest wavelength of the 4-Py-CHO ligand recorded in hexane solution by Ohno et al. was 283.3 nm [52]. It shifted to a longer wavelength after complexation, supporting the experimental finding and the coordination of 4-Py-CHO with the copper(I) ion.

The complex shows a moderately strong band at 300 nm with an intense band at 360 nm (Fig. 3). To explain the nature of electronic transitions in the title complex, TD-DFT calculations were performed on optimized geometries in DMSO. Calculated electronic

Table 2
Experimental and calculated UV-Vis wavelength (λ), band gap energy (eV) and oscillator strength for the Cu(I) complex.

Experimental (DMSO)		TD-DFT/CAM-B3LYP/DGDZVP Solvent phase (DMSO)			
λ_{max}(nm)	Band Gap (eV)	λ_{max}(nm)	Osc. Strength (f)	Excitation (eV)	Important orbital excitations
300	4.133	263	0.231	4.709	%53 ($H_{-6} \rightarrow$ LUMO)
360	3.444	332	0.318	3.735	%80 (HOMO $\rightarrow L_{+1}$)

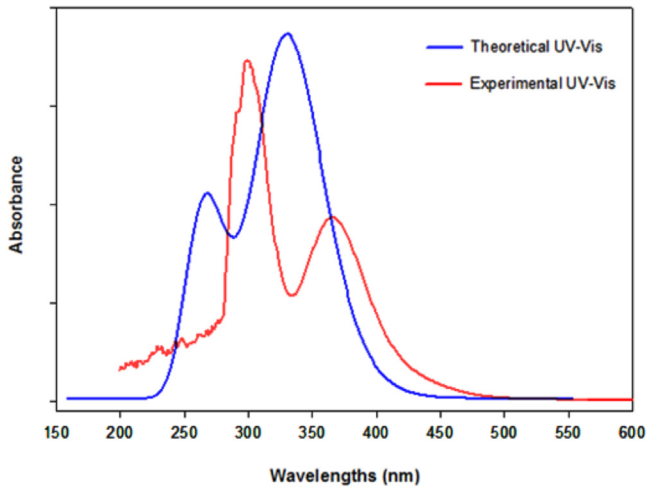

Fig. 3. The UV–vis spectrum of the Cu(I) complex was carried out experimentally and theoretically.

spectral data is intense band HOMO→LUMO+1 for the complex at 332 nm. The peak at 263 nm corresponds to HOMO-6→LUMO transitions having the $\pi \rightarrow \pi^*$ character. These transitions have the characteristics of intra-ligand charge transfer and metal-to-ligand charge transfer. Strong absorption bands were observed in copper (I) complexes, which were attributed to the ligand to metal charge transfer (LMCT) transition (N→Cu) [53].

The oscillator power f is a dimensionless quantity describing the power of an electronic transition, and the oscillator power for the theoretical transition was obtained differently in magnitude from the experimental transitions. The first reason may be related to the limitations of charge-transfer TD-DFT computations. The second reason is that the influence of the geometry of complex cannot be ignored. Theoretical calculations were done with utilizing optimized geometry, and experimental results for the bulk material were found.

4.4. AIM topological, reduced density gradient (RDG) and NBO analyses

The existing intermolecular interactions in the Cu(I) complex have been confirmed and analyzed theoretically using geometric optimization and AIM topological analysis, as well as through multi-wavefunction analysis, which was carried out via an RDG plot analysis and isosurface of contacts. Table 3 shows the calculated topological parameters. The weak hydrogen bonds are defined by $\nabla^2\rho(r) > 0$, $H(r) > 0$, $E_{bond} < 12.0$ kcal/mol, and they are mostly electrostatic, with a distance between interacting atoms higher than the total of their van der Waals rays [54,55]. According to this Table 3, positive Laplacian indicates the local depletion of electron density, typical of closed shell interactions, as it occurs in ionic bonds or any other interactions like van der Waals, weak hydrogen bonding, etc. Positive Laplacian values also imply depletion of electronic charge along the liaison path; the highest density found is for the C-H...N and C-H...I contacts, most likely due to the close proximity of those atoms. The energy of the hydrogen bond is calculated for our compound as around 6 kJ/mol. In our case, the appearance of a new ring critical point 'RCP' confirms the cyclic character of an atomic chain. As shown in Fig. 4, the interactions between the organic group and the $[CuI]^-$ anion via hydrogen bonds give rise to the formation of the rings NRCP1, NRCP2 and NRCP3. According to the AIM analysis, the Cu-N and Cu-I interactions are $\nabla^2\rho(r) > 0$ and $H(r) < 0$ implies that the H-bond is of medium-weak interaction, moderately covalent in nature, and the kinetic energy dominates. The Cu-N interaction has a higher electron density $\rho(r)$ value, which is corroborated by the fact that the Cu-I bond lengths computed in Table 1 are longer than the Cu-N2 and Cu-N45 bond lengths, which indicate that the Cu-N interactions are stronger than the Cu-I in the complex. The hydrogen bonds and coordination bonds in the title complex were easier to understand after the chemical bonds were broken down.

Jenkins and Morrison [56], and Espinosa et al. [57,58] proposed that bond interactions are sorted according to the $|V(r)|/G(r)$ ratio, the ratio $|V(r)|/G(r) < 1$, the bonded interaction is regarded as the closed shell, when $|V(r)|/G(r) > 2$, it is considered as the typically covalent interaction; and when $1 < |V(r)|/G(r) < 2$, it is the intermediate character. The mean $|V(r)|/G(r)$ ratio for the C–H···N and C–H···I interactions is less than 1.0, as shown in Table 3. As a result, these interactions are mostly the closed shell for the complex model. The typical $|V(r)|/G(r)$ ratio for Cu–N interactions is 1.21, which is somewhat higher than 1.0. As a result, for the complex model, the Cu-N interactions constitute the intermediary character between the closed-shell and the typically covalent interaction.

The non-covalent interaction (NCI) analysis provides crucial information regarding a molecule's non-covalent interactions. We have attempted to comprehend and show the nature of the intensity of the many interactions present in the title complex using the density $\rho(r)$ versus sign λ_2: If $\lambda_2 < 0$: Attractive and binding interactions (hydrogen bonds). $\lambda_2 > 0$ is greater than 0, repulsive and non-binding interactions occur (steric effect in ring and cage). Values close to zero indicate van der Waals interactions. As can be seen in Table 3, there is a spike in negative λ_2 in the low gradient, low density area, indicating a stabilizing interaction such as hydrogen bonding. The results are summarized in Fig. 5a and b demonstrate the attractive, van der Waals. and repulsive interactions that exist in our compound structure. Van der Waals interactions are responsible for the interactions that appear as green plates and are situated exactly between the Cu(I) ion and nitrogen atoms. The elliptic red plate located at the center of the aromatic nucleus is related to π-π stacking interactions between the pyridine rings and show a strong steric effect due to high repulsions [59]. The green plates signifie the strong attractive interaction C-H…N and C-H….I. The RDG peak at -0.01 corresponds to a strong interaction between nitrogen and hydrogen. These results are comparable to those found using the AIM approach.

It's useful to calculate the energy lost due to electron delocalization in H-bonding. NBO analysis confirms the existence of X-H…Y hydrogen bonds between the different interaction acceptor-donor. For example, the C-H…N and C-H….I bonding are viewed as an interaction between an occupied non-bonded natural orbital of the acceptor atom lone pair LP(N) and the unoccupied anti-bonding orbital of the donor (C) in the C-H bond, anti-bonding acceptor orbital σ^*(C-H). This interaction weakens and lengthens

Table 3
Topological parameters of hydrogen bonded interaction for Cu(I) complex.

Interactions	$\rho(r)$	$\nabla^2\rho(r)$	$H(r)$	$G(r)$	$V(r)$	$E_{bond}(kJ/mol)$	$\|V(r)\|/\ G(r)$	λ_1	λ_2	λ_3
Cu-I	0.03135	0.22168	-0.0004	0.10302	-0.06248	82.01	0.6064	-0.03114	-0.02955	0.27717
Cu- N_2	0.06914	0.42791	-0.0299	0.13690	-0.16683	218.96	1.2186	-0.10060	-0.09566	0.62418
Cu-N_{45}	0.06916	0.42800	-0.0299	0.13696	-0.16691	219.07	1.2186	-0.10065	-0.09570	0.62444
Cu-N_{46}	0.02461	0.00584	-0.0001	0.12080	-0.00118	1.54	0.0097	-0.00100	-0.00919	0.00776
C_{18}-H_{19}....N_1	0.00721	0.02394	0.00064	0.00534	-0.00469	6.15	0.8782	-0.00678	-0.00614	0.03687
C_{34}-H_{52}....N_1	0.00781	0.02614	0.00072	0.00581	-0.00509	6.68	0.8760	-0.00748	-0.00678	0.04041
C_{20}-H_{21}....N_{46}	0.00784	0.02623	0.00072	0.00583	-0.00510	6.69	0.8747	-0.00751	-0.00618	0.04056
C_{30}-H_{51}....N_{46}	0.00718	0.02385	0.00064	0.00532	-0.00467	6.13	0.8778	-0.00675	-0.00611	0.03672
C_3-H_{50}....I	0.00737	0.02423	0.00062	0.00542	-0.00480	6.31	0.8856	-0.00541	-0.00491	0.03455
C_{27}-H_{28}....I	0.00737	0.02424	0.00063	0.00543	-0.00480	6.31	0.8839	-0.00541	-0.00491	0.03457

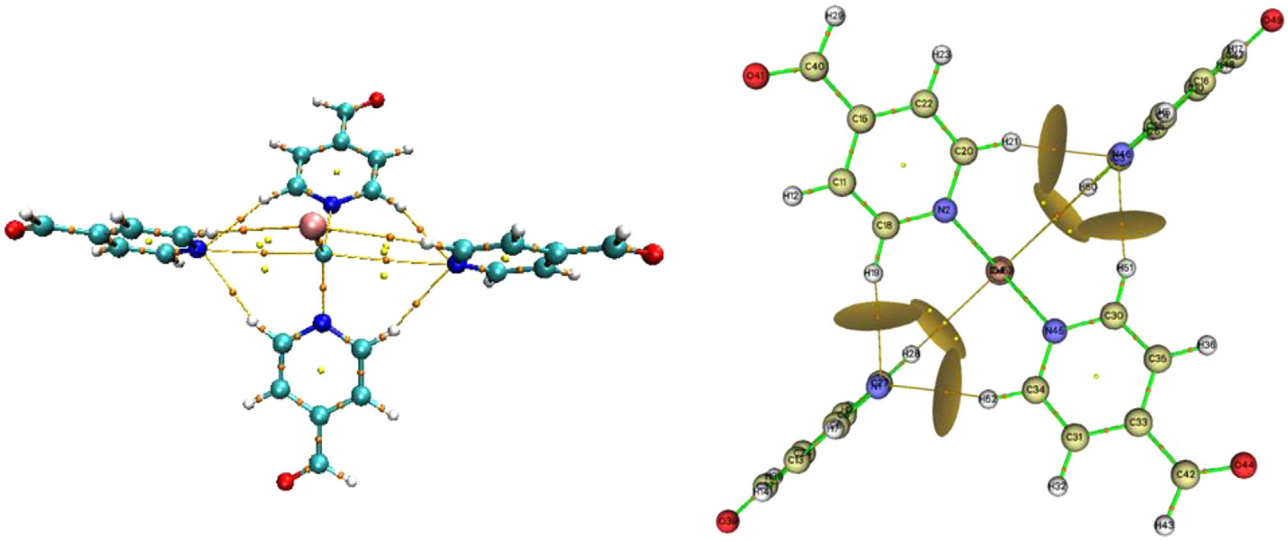

Fig. 4. AIM molecular graphic showing the different critical points of Cu(I) complex.

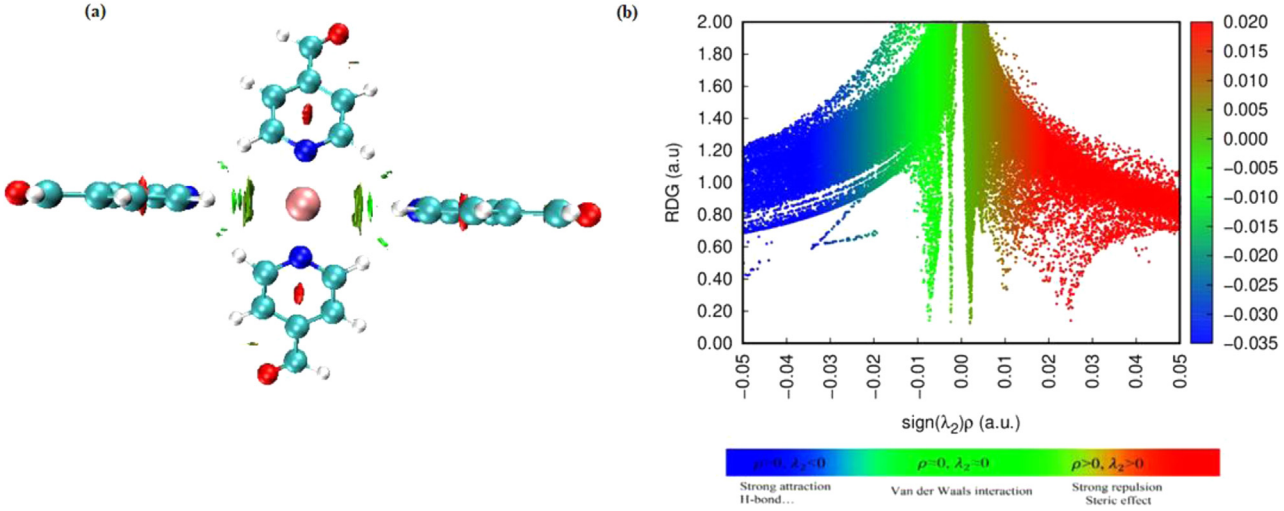

Fig. 5. Representation of different types of interactions in Cu(I) complex (a). The map of reduced density gradient (RDG) defines the interaction limits for complex (b).

the C-H bond, thus leading to red-shifted stretching frequency of C-H bond. The interaction between electron donor and acceptor is more intense if the stabilization energy $E^{(2)}$ is larger [60]. The larger value of total stabilization energy for C_{20}-H_{21}....N_{46} and C_{34}-H_{52}....N_1 interaction indicates it is stronger than others, being also consistent with the longer C-H bond lengths. The C-H....N is having the least stabilization energy of 2.65 kcal/mol lower than the C-H....I. These results are consistent with AIM analysis.

The computed second order interaction energy $\boldsymbol{E}^{(2)}$ of Metal-Ligand bonds in the examined complex is listed in Table 4. The stronger the contact between electron donors and electron acceptors, the higher the $\boldsymbol{E}^{(2)}$values. Table 4 clearly demonstrates that the interaction energy between each metal ion and the iodine atom is greater than the interaction energy between metal ions and nitrogen atoms. The maximum energy $\boldsymbol{E}^{(2)}$ value for the copper complex was 19.90 kcal/mol, which corresponds to LP(1) N→ LP*(8) Cu. Electron donation from the filled lone pair donor NBOs

Table 4
Second-order perturbation theory analysis of Fock matrix in NBO corresponding to the selected charge transfer interactions of the complex.

H-bonds	*donor→acceptor*	$E^{(2)}$ *(kcal/mol)*[a]	$\varepsilon_j - \varepsilon_i$ *(a.u.)*[b]	$F(i,j)$ *(a.u.)*[c]	*C-H (Å)*
C_{18}-H_{19}....N_1	$LP(1)(N_1) \rightarrow \sigma^*(C_{18} - H_{19})$	0.86	0.79	0.024	1.0847
C_{34}-H_{52}....N_1	$LP(1)(N_1) \rightarrow \sigma^*(C_{34} - H_{52})$	2.52	0.79	0.026	1.0845
C_{20}-H_{21}....N_{46}	$LP(1)(N_{46}) \rightarrow \sigma^*(C_{20} - H_{21})$	2.65	0.66	0.030	1.0845
C_{30}-H_{51}....N_{46}	$LP(1)(N_{46}) \rightarrow \sigma^*(C_{30} - H_{51})$	0.85	0.66	0.023	1.0847
C_3-H_{50}....I	$LP(3)(I_{54}) \rightarrow \sigma^*(C_3 - H_{50})$	1.29	0.65	0.036	1.0868
C_{27}-H_{28}....I	$LP(3)(I_{54}) \rightarrow \sigma^*(C_{27} - H_{28})$	1.23	0.65	0.036	1.0868
Metal-ligand bonds	***donor→acceptor***	$E^{(2)}$ *(kcal/mol)*[a]	$\varepsilon_j - \varepsilon_i$ *(a.u.)*[b]	$F(i,j)$ *(a.u.)*[c]	
	$LP(1)(N_2) \rightarrow LP^*(8)(Cu_{53})$	16.59	0.65	0.0118	
	$LP(1)(N_{45}) \rightarrow LP^*(8)(Cu_{53})$	19.90	0.66	0.104	
	$LP(1)(N_{46}) \rightarrow LP^*(7)(Cu_{53})$	0.19	0.01	0.012	
	$LP(1)(I_{54}) \rightarrow LP^*(6)(Cu_{53})$	11.19	0.36	0.185	

σ : sigma bonds, π : pi bonds, *LP*: lone pairs, LP*: anti-lone pairs
[a] $E^{(2)}$ means energy of hyper conjugative interactions.
[b] Energy difference between donor and acceptor i and j NBO orbitals.
[c] $F_{(i,j)}$ is the Fock matrix element between i and j NBO orbitals

Table 5
Selected atom net NBO (natural bond orbital) charges and electronic configuration of the complex.

Atom	*Charge (e)*	*Electron configuration*
Cu	0.54701	[core]$4s^{0.33}3d^{9.83}4p^{0.29}4d^{0.01}$
I	-0.63930	[core]$5s^{1.93}5p^{5.71}5d^{0.01}$
N1	-0.47343	[core]$2s^{1.38}2p^{4.07}3d^{0.01}4p^{0.01}$
N2	-0.51287	[core]$2s^{1.34}2p^{4.14}4p^{0.02}$
N45	-0.47344	[core]$2s^{1.34}2p^{4.14}4p^{0.02}$
N46	-0.53088	[core]$2s^{1.38}2p^{4.108}$ $3p^{0.01}$ $3d^{0.01}4p^{0.01}$
O39	-0.50806	[core]$2s^{1.70}2p^{4.79}3p^{0.01}$
O41	-0.50445	[core]$2s^{1.70}2p^{4.79}3p^{0.01}$
O44	-0.50444	[core]$2s^{1.70}2p^{4.79}3p^{0.01}$
O49	-0.50805	[core]$2s^{1.70}2p^{4.78}3p^{0.01}$

of the I and N atoms to the empty metal hybrid orbitals might be characterized as the acceptor-donor interactions. The second lone pair of N atoms is responsible for the crucial interactions with the anti-bonding NBOs of the Cu ion, according to an analysis of the ligand groups' natural orbitals.

The natural atomic charges and natural electron configurations of the Cu, I, N, and O atoms of the complex obtained from NBO analysis are listed in Table 5. As shown in Table 5, the most important interactions are between iodine and nitrogen non-bonding lone-pairs as donors orbitals of copper as acceptors. Copper has a net charge of 0.547 e, whereas free copper(I) ion has a valence of +1. The valence of free iodide atoms, on the other hand, is −1, whereas their net charge in the complex is 0.639e. It shows that a significant amount of charge density on the central atom is transferred from the ligand fragment to the copper central metal. The reduction in the net charge of the iodine atom leads to the conclusion that during complexation, copper(I) obtains electron density from the iodine atom. Also, the charge on the copper ion has also been reduced from its normal value as a result of its involvement in complexation with the ligand, which has been reduced in the previous complex studies [61].

4.4. Molecular reactivity analyses

Frontier molecular orbitals (FMO's) are important factors in quantum chemistry computations. The MO's analysis has an important role in electrical, optical, and chemical reactions [62], and also helps to establish the chemical reactivity and kinetic stability of compounds [63]. Fig. 6 illustrates the HOMO and LUMO, while their quantum chemical parameters are listed in Table 6. As seen in Fig. 6, the LUMO is delocalized over the π^* system of the nitrogen-donating ligand. On the other hand, the HOMO is mainly localized over the Cu(I) and iodine atom. The molecular orbital analysis is used to forecast the NBO's, which are related to donor-acceptor interactions [33]. All interactions between copper(I) atoms and coordinating atoms are referred to as coordinate bonds of the type Cu-N or Cu-I in molecular orbital analysis. In these interactions, electron density is transferred from the nitrogen or iodide atoms' lone pair orbitals, LP(N) or LP(I), to the antibonding LP* (Cu). These distributions are also supported by the HOMO-LUMO surfaces shown in Fig. 6.

The energy gaps between the HOMO-LUMO orbitals are critical characteristics for determining the electrical transport of the compound, and the chemical potential, electrophilicity index, hardness, and softness of molecules were estimated using these energy values given in Table 6. These parameters are used to analyze biological characteristics and to recognize active sites [64]. The HOMO-LUMO energy gap of the copper(I) iodide complex (E = 4.81 eV) similar studies [65,66] reported that the structure has bioactivity at values close to this energy range. In addition to the E_{gap} value, chemical hardness and negative chemical potential also provided chemical stability of the compound. As shown in Table 6, the chemical hardness value is greater than the softness value, which indicates the chemical stability of the material. Also, chemical hardness is a good index to estimate the chemical strength of the compounds [32]. The title complex found, with an extremely low chemical softness value of 0.21, was therefore considered to be non-toxic and highly biological active [67,68]. The lower values of the HOMO-LUMO energy gap and the high electrophilicity index have a significant effect on the binding affinity while at the same time indicating the biological presence of the compound.

4.9.1. Total partial and overlap population density-of-states

To understand the orbital compositions of the different MOs in the complexes, the partial, total, and overlap population density of states (PDOS, TDOS, and OPDOS) were plotted for all cluster interactions [69]. The left side axis correlates to TDOS and PDOS, while the right side axis refers to OPDOS, and the vertical dashed line emphasizes the HOMO position. The PDOS graphic primarily depicts the contribution of fragment orbital compositions to molecular orbitals. The HOMO molecular orbital has both bonding and antibonding interactions, while the LUMO molecular orbital only has antibonding interactions. As seen in Fig. 7, PDOS results of the complex revealed that the main contributions to HOMO orbitals were of iodide and copper(I) fragments. However, the LUMO molecular orbital contributions of nitrogen of the pyridine ring were more significant than those of the other fragments. This concurs with the HOMO and LUMO diagrams presented.

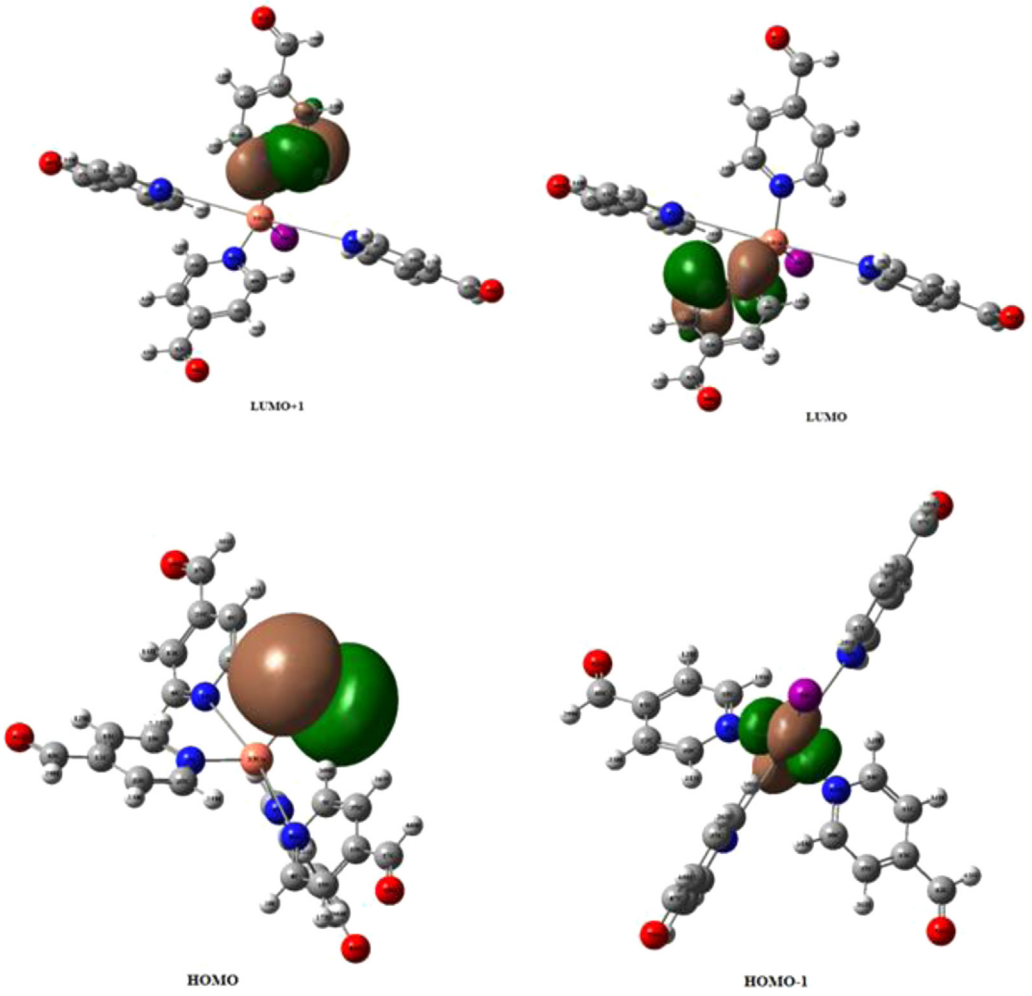

Fig. 6. HOMO and LUMO surfaces of copper(I) iodide complex.

Table 6
Global reactivity descriptors of the copper(I) iodide complex.

Energy gap (eV)	Ionization potential (I)(eV)	Electron affinity (A)(eV)	Global hardness (η)(eV)	Electronegativity (χ)(eV)	Chemical potential (μ_c)(eV)	Global softness (σ)(eV) $^{-1}$	Global electrophilicity (ω)(eV) $^{-1}$	Maximum charge transfer index(ΔN_{max})
4.81	6.01	1.20	2.40	3.61	-3.61	0.21	2.73	1.56

H: HOMO, L: LUMO
I= -E_{HOMO}, A= -E_{LUMO}, $\eta = \frac{(I-A)}{2}$, $\mu = \frac{-(I+A)}{2}$, $\chi = \frac{(I+A)}{2}$, $\sigma = \frac{1}{2\eta}$, $\omega = \mu^2/2\eta$, $\Delta N_{max} = -\mu/\eta$

4.6. MEP (Molecular electrostatic potential) analysis

MEP analysis is used to predict the chemical reactive behavior of a wide range of chemical materials in biological systems, including nuclophilic and electrophilic reactions, enzyme-substrate interactions, and hydrogen bonding interactions [70]. The MEP is a colour-coded depiction of the predicted electron density surface; red, blue, and green represent negative, positive, and neutral electrostatic areas, respectively. In the present work, an analysis of the nucleophilic and electrophilic attack sites of the title complex is presented in Fig. 8. It is clear from Fig. 8, the most positive region represented by blue colour are related to nucleophilic reactivity is around –CH proton. Also, the ionic copper located at the central position of the positive electrostatic region. According to the MEP analysis, the Cu(I) complex appears to have a high positive electrostatic potential distributed over its skeleton. On the other hand, the negative potentials are over the electronegative O atoms belonging to the carbonyl groups of ligands and electrophilic are located near iodine. These negative regions, which are shown in red, show electrophilic reactivity. These reactive sites appearing on the MEP are favorable for H-bond interaction with selected proteins in molecular docking investigations. The dispersion of potential in the Cu(I) complex ranges from -0.4384e-2 to 0.4384e-2.

4.7. Thermal Analysis of the synthesized complex

The TGA thermogram of title complex shown in Fig. S2 displays a four-step decomposition pattern of the Cu(I) complex. The first step observed between 100 and 250 °C shows a mass loss of 27.96% corresponding to the decomposition of the O-H and C=O groups. The second weight loss between 240 and 270 °C can be assigned to the decomposition of the complex by 10%. The third step takes place between 270 and 300 °C which loses the mass of 40%, which is defined by the removal of pyridine rings. In the last step, the remainder of the complex was decomposed, which represents 10.3% of the mass.

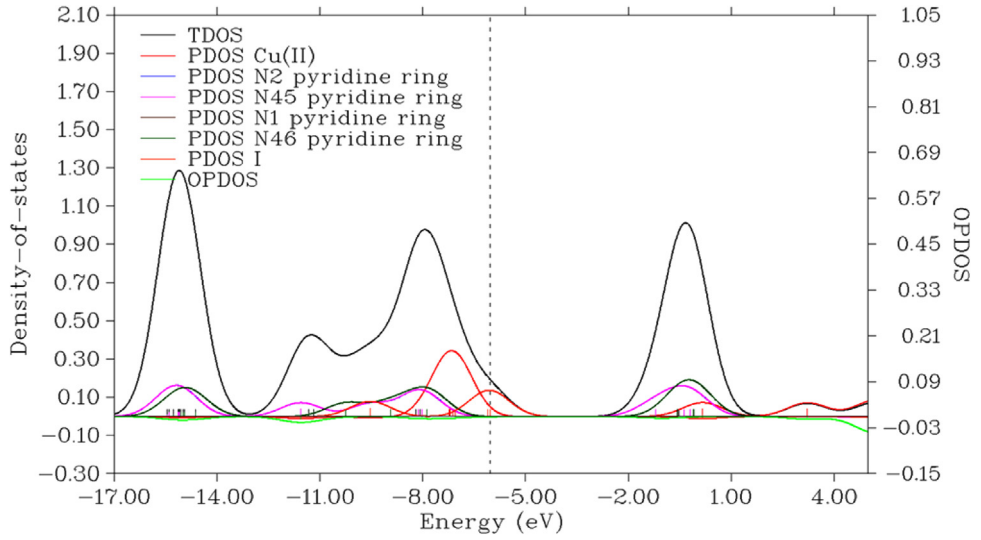

Fig. 7. The calculated PDOS, TDOS and OPDOS Plots for Cu(I) complex.

Table 7
The minimum inhibitory concentration (MIC) and the diameter of the inhibition zone define the antibacterial activity of Cu(I) complex (mm).

Test Bacteria	DIZ (mm)	MIC (μg/ml)	AMP (10 μg)	10% DMSO
S. aureus ATCC 29213	15.2	7.81	18	-
S. epidermidis ATCC 35984	13.2	7.81	16	-
L.monocytogenes ATCC 35152	-	-	15	-
B. subtilis ATCC 6633	-	-	12	-
B. cereus 709 Roma	-	-	12	-
E. faecalis ATCC 29212	-	-	18	-
E. coli ATCC 25922	-	-	18	-
S.typhimurium ATCC 14028	-	-	16	-
P. aeruginosa ATCC 27853	-	-	16	-
K. pneumoniae ATCC 13883	-	-	15	-
C. violaceum ATCC12472 (Antiquorum-sensing activities)	12	-	-	-

MIC (μg/ml): Minimum Inhibitory Concentration, DIZ (mm): Diameter of inhibition zone (mm), Positive control: AMP (10μg): Ampicillin, Negative control: 10% DMSO. Note: – indicates no inhibition

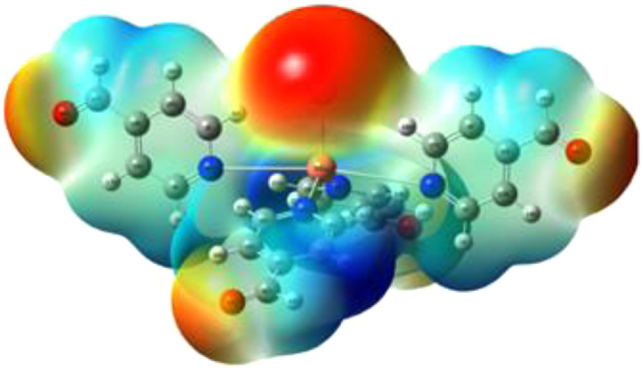

Fig. 8. Molecular electrostatic potential map of the copper(I) complex.

5. Biological properties

5.1. Antibacterial and antiquorum-sensing screening activity

Table 7 shows the antibacterial activity of the chemical based on Minimal Inhibitory Concentration (MIC) and zone of inhibition diameter (mm).

[CuI(4-Py-CHO)$_4$] showed good antibacterial activity against *S. aureus* and *S. epidermidis* (MIC: 7.81 µg / mL). The antibacterial activity was measured using agar well diffusion.

When Gram positive bacteria (*S. aureus* and *S. epidermidis)* were diluted in DMSO (10 mg/ml), they showed good sensitivity to Cu(I) iodide complex, with inhibitory zone diameters of 15.2 and 13.2 mm, respectively (Table 7).

The results were compared to those of the common antibiotic ampicillin. According to the findings, the title chemical has high to moderate antibacterial activity against all of the species tested. The title compound did not show antibacterial activity in Gram negative bacteria.

Quorum-sensing mechanisms in bacteria have a focus on microbial resistance mechanisms and microbial biofilm production regulation. These results emphasize the possibility for the Cu(I) complex to be developed as an antibacterial treatment for infections linked to biofilms. To prevent microbial resistance, a new technique for treating proposed drug-resistant microorganisms can be devised employing QS [71]. The purple pigment violacein is produced by *C. violaceum* and is controlled by acyl HSL-mediated QS. As a result, drugs that inhibit acyl HSL-mediated QS activity in C. violaceum will also inhibit purple pigment production [72].

Therefore, Cu(I) complex was examined for their antiquorum-sensing activities against *C. violaceum.* In our study, the titled compound was found to be capable of inhibiting the production of violacein pigment in *C. violaceum* (Table 7).

5.2. Molecular docking

Molecular docking studies are carried out to complement pharmacological data [73] and give biological support for biological activity. It shows how drug candidates interact with target proteins in the binding site [74].

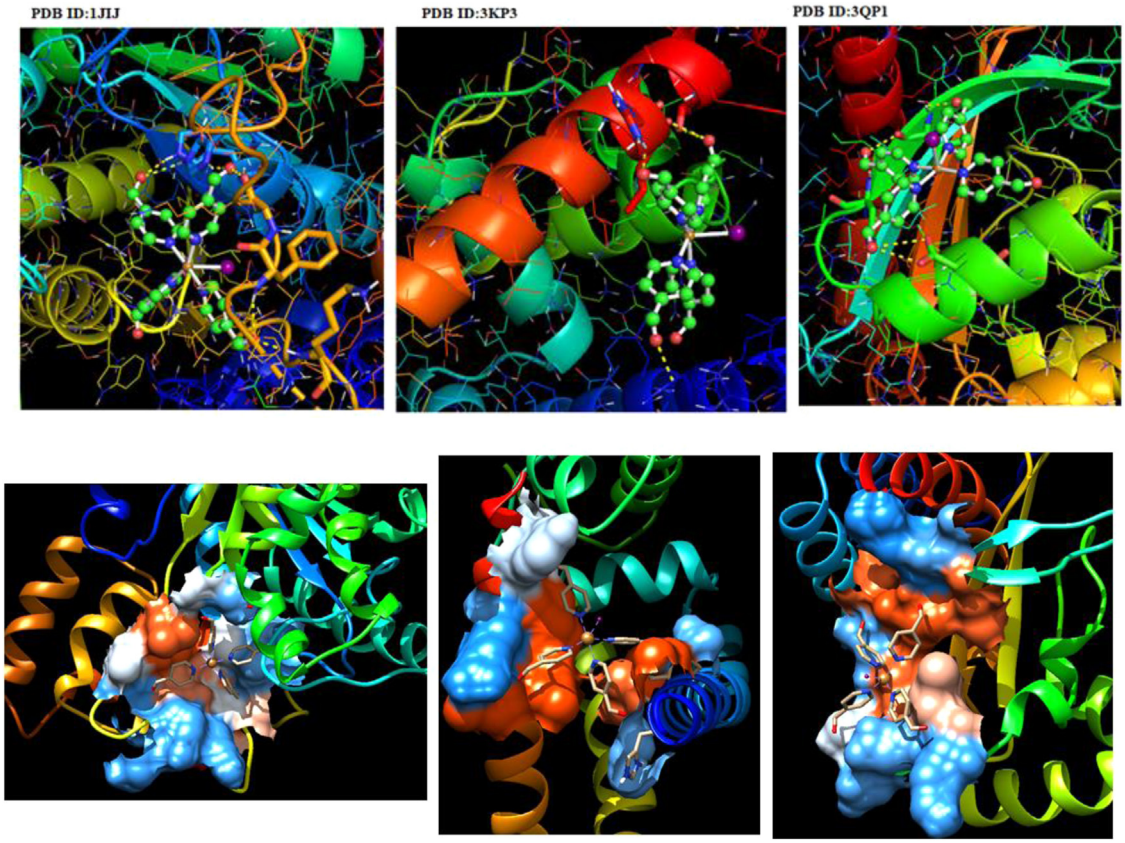

Fig. 9. Binding interaction and binding residues of receptor protein Cu(I) complex.

In this study, the *in vitro* antibacterial activity of the synthesized complex was experimentally confirmed. To confirm this, an insilico molecular docking computational approach was employed to provide an excellent basis for the drug design to treat bacterial diseases. Therefore, bacterial receptors (1JIJ, 3KP3, and 3QP1) were selected for molecular docking. The in-silico molecular docking results given in Table S2, the binding energy of all proteins is negative and this value shows that the molecule is linked to a protein [75]. The *S.aureus* protein (1JIJ) is the strongest inhibitor in binding energy at -8.73 kcal/mol, indicating that the higher the binding energy, the more sturdy the interaction [76], and the best docked state has an intermolecular energy of -10.92 kcal/mol. The more negative the numerical value of binding energy parameter, the higher the biological activity of the molecule and the greater the interaction between molecules and proteins. They demonstrate that the higher the interaction, the more the bond rigidity sinks, and their prominent RMSD value of 78.16. Furthermore, the low binding energy value obtained indicates that the title Cu(I) compound is biologically active [67]. Theoretically, the synthesized complex gave a good docking score and binding energy to the particular protein targets.

Intermolecular hydrogen bonding between the title complex and the proteins is shown in Fig. 9. According to the protein–ligand interaction major contribution, a hydrogen bond is formed between the oxygen atoms in the C=O in the ligand and the hydrogen atom in the chosen antibacterial proteins. For example, the oxygen atom of the aldehyde group was hydrogen-bonded with the hydrogen atoms (NH) of HIS'50 (d = 2.19 Å), ARG'143 (d = 1.83 Å), ASN'77 (d = 1.88 Å). Additionally, this interaction reveals the formation of amino acid residues HIS50, HIS47, LYS226, PHE232, and VAL240 via the H-bond interaction NH—O and results in increased hydrophobic energy contributions in the ligand due to higher binding energy values. On the other hand. Cu(I) complex made attractive and noncovalent Pi-Sigma and Pi-Alkyl interactions between the pyridine ring of this compound and the residues.

Food poisoning, infections, and sepsis are all caused by *Staphylococcus aureus*, a bacterial pathogen. Antibiotic resistance has risen rapidly in recent years, necessitating the development of new medications and effective techniques to combat infections caused by S. *aureus*. In this case, the headline copper complex, which has antibacterial properties against *S.aureus*, is a promising precursor compound for new pharmaceutical research. It can also be used as a disinfectant candidate. These findings will aid in the development of more effective, faster mechanisms of action of the title compound in designing new potential antibacterial drugs.

Ramachandran plots were calculated using PROCHECK [77] to validate the stereochemical quality of modelled protein structures. The Ramachandran plot for three docked target proteins portrayed the Psi/Phi angle distribution in Fig. S3 demonstrates that 90% of the amino acids lie in the allowed region, which is indicated by the red color, and only a very few lie in the disallowed region, which indicates the stability of the protein chosen for the binding interaction. The identified protein molecules are structurally stable, as shown by the Ramachandran plot.

6. Conclusion

In the present paper, the novel synthesized Cu(I) complex optimized structural parameters, electronic, topological, and vibrational analysis were investigated using the DFT method. Chemical bonding, antibonding interactions, and stabilization energy have all been investigated using donor-acceptor analysis. These data aided in the prediction of reactivity and the identification of the complex's active site. The Cu complex exhibited significant antibacterial activity against *S. aureus* and *S. epidermidis* with biofilm and quorum sensing properties. As a result, the Cu(I) metal complex

demonstrated only bacteriocidal activity against *S. aureus and S. epidermidis*. As a result, we believe the copper(I) iodide complex can aid in the development of new synthetic antibiotics and antiseptics. Most active drugs have excellent interaction score values, according to the molecular docking studies. The purpose of this study is to investigate the in silico and *in vitro* bioactivity of manufactured chemicals to determine whether they have antibacterial properties. The binding affinity of the synthesized complex towards the antibacterial proteins supports the compound's antibacterial activity to treat bacterial diseases. The results of topological analyses of the title chemical complement those obtained from molecular docking studies. Clearly, quantum chemical parameters with MEPs can accurately describe compound biological activity.

Declaration of Competing Interest

The authors declare that they have no known competing financial interests or personal relationships that could have appeared to influence the work reported in this paper.

CRediT authorship contribution statement

Sibel Celik: Conceptualization, Data curation, Investigation, Methodology, Software, Supervision, Validation, Visualization, Writing – original draft. **Senay Yurdakul:** Conceptualization, Data curation, Methodology, Supervision, Validation, Writing – original draft. **Belgin Erdem:** Conceptualization, Data curation, Methodology, Validation, Writing – original draft.

Data Availability

No data was used for the research described in the article.

References

[1] N.H. Campbell, N.H.A. Karim, G.N. Parkinson, M. Gunaratnam, V. Petrucci, A.K. Todd, R. Vilar, S. Neidle, Molecular basis of structure-activity relationships between salphen metal complexes and human telomeric DNA quadruplexes, J. Med. Chem. 55 (1) (2012) 209–222.

[2] D. Inci, R. Aydın, O. Vatan, T. Sevgi, D. Yılmaz, Y. Zorlu, Y. Yerli, B. Cosut, E. Demirkan, N. inkılıc, Synthesis and crystal structures of novel copper(II) complexes with glycine and substituted phenanthrolines: reactivity towards DNA/BSA and *in vitro* cytotoxic and antimicrobial evaluation, J. Biol. Inorg. Chem. 22 (1) (2017) 61–85.

[3] D. Inci, R. Aydın, H. Huriyet, O. Vatan, Y. Zorlu, B. Cosut, N. inkılıc, Cu(II) tyrosinate complexes containing methyl substituted phenanthrolines: synthesis, X-ray crystal structures, biomolecular interactions, antioxidant activity, ROS generation and cytotoxicity, Appl. Organomet. Chem. 33 (1) (2019) e4652.

[4] Z.C. Liu, B.D. Wang, B. Li, Q. Wang, Z.Y. Yang, T.R Li, Y. Li, Crystal structures, DNA-binding and cytotoxic activities studies of Cu(II) complexes with 2-oxo-quinoline-3-carbaldehyde Schiff-bases, Eur. J. Med. Chem. 45 (11) (2010) 5353–5361.

[5] D.H. Cai, C.L. Zhang, Q.Y. Liu, L. He, Y.J. Liu, Y.H. Xiong, X.Y. Le, Synthesis, DNA binding, antibacterial and anticancer properties of two novel water-soluble copper(II) complexes containing gluconate, Eur. J. Med. Chem. 213 (2021) 113182.

[6] N.K. Singh, A.A. Kumbhar, Y.R. Pokharel, P.N. Yadav, Anticancer potency of copper(II) complexes of thiosemicarbazones, J.Inorg. Biochem. 210 (2020) 111134.

[7] S.K.M. Muslim, M. Ahmad, M. Arish, M. Jane Alam, A.K. Pradhan, P. Mondal, A. Alarifi, M. Afzal, Structural elucidation and cytotoxicity profile of neocuproine-Cu(II) and Cu(I)-based chemotherapeutic agents: effect of picric acid-derived cocrystals, Polyhedron 220 (2022) 115848.

[8] A. Ali, N. Sepay, M. Afzal, N. Sepay, A. Alarifi, M. Shahid, M. Ahmad, Molecular designing, crystal structure determination and in silico screening of copper(II) complexes bearing 8-hydroxyquinoline derivatives as anti-COVID-19, Bioorgan. Chem. 110 (2021) 104772.

[9] Z.C. Liu, B.D. Wang, B. Li, Q. Wang, Z.Y. Yang, T.R. Li, Y. Li, Crystal structures, DNA-binding and cytotoxic activities studies of Cu(II) complexes with 2-oxo-quinoline-3-carbaldehyde Schiff-bases, Eur. J. Med. Chem. 45 (2010) 5353–5361.

[10] R. Alizadeh, M. Afzal, F. Arjmand, In vitro DNA binding, pBR322 plasmid cleavage and molecular modeling study of chiral benzothiazole Schiff-base-valine Cu(II) and Zn(II) complexes to evaluate their enantiomeric biological disposition for molecular target DNA, Acta Part A Mol. Biomol. Spectrosc. 131 (2014) 625–635.

[11] N.L. Poul, M. Campion, B. Douziech, Y. Rondelez, L.L. Clainche, O. Reinaud, Y.L. Mest, Monocopper center embedded in a biomimetic cavity: from supramolecular control of copper coordination to redox regulation, J. Am. Chem. Soc. 129 (2007) 8801–8810.

[12] G.T. Musie, X.B. Li, D.R. Powell, Synthesis, crystal structure and redox properties of bis-imidazolyl-containing copper(II) complexes, Inorg. Chim. Acta 348 (2003) 69–74.

[13] D.D. Qin, Z.Y. Yang, F.H. Zhang, B. Du, P. Wang, T.R. Li, Evaluation of the antioxidant, DNA interaction and tumor cell cytotoxicity activities of Copper(II) complexes with Paeonol Schiff-base, Inorg. Chem. Commun. 13 (2010) 727–729.

[14] A.F. Crespi, V.M.S ´Anchez, D. Vega, A.L. Perez, C.D. Brondino, Y.G. Linck, P. Hodgkinson, E. Rodriguez-Castellon, J.M. Lazaro-Martinez, Paramagnetic solid-state NMR assignment and novel chemical conversion of the aldehyde group to dihydrogen ortho ester and hemiacetal moieties in copper(II)- and cobalt(II)-pyridinecarboxaldehyde complexes, RSC Adv. 11 (2021) 20216–20231.

[15] K. Nomiya, K. Tsuda, T. Sudoh, M. Oda, Ag(I)-N bond-containing compound showing wide spectra in effective antimicrobial activities: Polymeric silver(I) imidazolate, J. Inorg. Biochem. 68 (1997) 39–44.

[16] A. Martin, B. Lucke, H.J. Niclas, A. Forster, Vapor-phase oxidation of 4-picoline to pyridine-4-carboxaldehyde on a vanadium phosphate catalysts, React. Kinet. Catal. Lett. 43 (2) (1991) 583–588.

[17] N.K. Singh, R. Tripathi, Synthesis and structural characterization of 3d-metal complexes of pyridine-4-carboxaldehyde thionicotinoyl hydrazone, Trans. Metal Chem. 13 (5) (1988) 346–350.

[18] L. Cluyts, A. Sharma, N. Kuş, K. Schoone, R. Fausto, Matrix isolation infrared spectroscopic study of 4-Pyridinecarboxaldehyde and of its UV-induced photochemistry, Spectroc. Acta Part A Mol. Biomol. Spectroc. 171 (2017) 207–212.

[19] H. Kargar, R. Behjatmanesh-Ardakani, V. Torabi, M. Kashani, Z. Chavoshpour-Natanzi, Z. Kazemi, V. Mirkhani, A. Sahraei, M. Nawaz Tahir, M. Ashfaq, K.S. Munawar, Synthesis, characterization, crystal structures, DFT, TD-DFT, molecular docking and DNA binding studies of novel copper(II) and zinc(II) complexes bearing halogenated bidentate N,O-donor Schiff base ligands, Polyhedron 195 (2021) 114988.

[20] B.J. McConkey, V. Sobolev, M. Edelman, The performance of current methods in ligand-protein docking, Curr. Sci. 83 (2002) 845–855.

[21] V. Sivaa, A. Chitra Devi, S. Thangarasu, T.M. Viswanathan, S. Athimoolam, S. Asath Bahadur, Design, structural, DFT, molecular docking studies and biological evaluation of 4-aminiumantipyrine dihydrogenphosphate monohydrate, J. Mol. Struct. 1250 (2022) 131866.

[22] NCCLS. Performance Standards for Antimicrobial Susceptibility Testing: 10th Informational Supplement (Aerobic Dilution, MIC Testing Supplemental Tables. NCCLS document M100-S10 (M7), supplement to NCCLS document M7-A5 (MIC testing); 2000.

[23] NCCLS. Performance Standards for Antimicrobial Susceptibility Testing: 13th Informational Supplement (Disk Diffusion Supplemental Tables). NCCLS document M100-S13 (M2), supplement to NCCLS document M2-A8 (disk diffusion); 2003.

[24] M. J. Frisch, G. W. Trucks, H. B. Schlegel, G. E. Scuseria, M. A. Robb, J. R. Cheeseman, G. Scalmani, V. Barone, B. Mennucci, G. A. Petersson, H. Nakatsuji, M. Caricato, X. Li, H. P. Hratchian, A. F. Izmaylov, J. Bloino, G. Zheng, J. L. Sonnenberg, M. Hada, M. Ehara, K. Toyota, R. Fukuda, J. Hasegawa, M. Ishida, T. Nakajima, Y. Honda, O. Kitao, H. Nakai, T. Vreven, J. A. Montgomery, Jr., J. E. Peralta, F. Ogliaro, M. Bearpark, J. J. Heyd, E. Brothers, K. N. Kudin, V. N. Staroverov, R. Kobayashi, J. Normand, K. Raghavachari, A. Rendell, J. C. Burant, S. S. Iyengar, J. Tomasi, M. Cossi, N. Rega, J. M. Millam, M. Klene, J. E. Knox, J. B. Cross, V. Bakken, C. Adamo, J. Jaramillo, R. Gomperts, R. E. Stratmann, O. Yazyev, A. J. Austin, R. Cammi, C. Pomelli, J. W. Ochterski, R. L. Martin, K. Morokuma, V. G. Zakrzewski, G. A. Voth, P. Salvador, J. J. Dannenberg, S. Dapprich, A. D. Daniels, O. Farkas, J. B. Foresman, J. V. Ortiz, J. Cioslowski and D. J. Fox, Gaussian, Inc., Wallingford CT, 2009.

[25] V. Devi, P. Awasthi, Synthesis, structural, DFT and bio-assay of novel ethyl 3-(2-(4-chlorophenoxy)acetamido) propanoate on Galleria mellonela (wax moth) – a juvenile hormone mimic as potential insect growth regulator (IGR), J. Mol. Struct. 1248 (2022) 131464.

[26] P. Pulay, J. Baker, K. Wolinski, Parallel Quantum Solut. 2013 Green Acres Road, Suite A, Fayetteville, AR 72703.

[27] R. Dennington, T. Keith, J. Millam, GaussView, Version 5, Semichem Inc., Shawnee Mission, KS, 2009.

[28] T. Lu, F. Chen, Multiwfn: a multifunctional wavefunction analyzer, J. Comput. Chem. 33 (2012) 580–592.

[29] W. Humphrey, A. Dalke, K. Schulten, VMD: visual molecular dynamics, J. Mol. Graph. 14 (1996) 33–38.

[30] W.L. DeLano Pymol: an open-source molecular graphics tool. CCP4 Newsletter on protein crystallography, 40 (2002) 82.

[31] T.D. Goddard, C.C. Huang, T.E. Ferrin, Visualizing density maps with UCSF chimera, J. Struct. Biol. 157 (1) (2007) 281–287 [Medline: 16963278, doi:10.1016/j.jsb.2006.06.010.

[32] H. Kargar, M. Ashfaq, M. Fallah-Mehrjardi, R. Behjatmanesh-Ardakani, K. Shahzad Munawar, M.N. Tahir, Synthesis, characterization, SC-XRD, HSA and DFT study of a novel copper(I) iodide complex with 2-(thiophen-2-yl)-4,5-dihydro-1H-imidazole ligand: an experimental and theoretical approach, J.Mol. Struct. 1253 (2022) 132264.

[33] Y. Singh, R.N. Patel, S.K. Patel, A.K. Patel, N. Patel, R. Singh, R.J. Butcher, J.P. Jasinski, A. Gutierrez, Experimental and quantum computational study of two new bridged copper(II) coordination complexes as possible models for antioxidant superoxide dismutase: molecular structures, X-band electron para-

magnetic spectra and cryogenic magnetic properties, Polyhedron 171 (2019) 155–171.
[34] S. Esmaielzadeh, E. Zarenezhad, Copper(II) Schiff Base complexes with catalyst property: experimental, theoretical, thermodynamic and biological studies, Acta Chim. Slov. 65 (2018) 416–428.
[35] A. Aguirrechu-Comeron, R. Hernandez-Molina, P. Rodriguez-Hernandez, A. Munoz, U.R. Rodriguez-Mendoza, V. Lavin, R.J. Angel, J. Gonzalez-Platas, xperimental and *ab Initio* Study of Catena(bis(μ_2-iodo)-6-methylquinoline-copper(I)) under Pressure: Synthesis, Crystal Structure, Electronic, and Luminescence Properties, Inorg. Chem. 55 (2016) 7476–7484.
[36] J.C. Li, H.X. Li, H.Y. Li, W.J. Gong, J.P. Lang, Ligand Coordination Site-Directed Assembly of Copper(I) Iodide Complexes of ((Pyridyl)-1-pyrazolyl)pyridine, Cryst. Growth Des. 16 (2016) 1617–1625.
[37] J. Conesa-Egea, J. Gallardo-Martinez, S. Delgado, J.I. Martinez, J. Gonzalez–Platas, V. Fernandez-Moreira, U.R. Rodriguez-Mendoza, P. Ocon, F. Zamora, P. Amo-Ochoa, Multistimuli Response Micro- and Nanolayers of a Coordination Polymer Based on Cu_2I_2 Chains Linked by 2-Aminopyrazine, Small (2017) 13–23.
[38] S. Celik, S. Yurdakul, B. Erdem, New silver(I) complex as antibiotic candidate: synthesis, spectral characterization, DFT, QTAIM and antibacterial investigations and docking properties, J. Mol. Struct. 1261 (2022) 132902.
[39] S.S. Margreat, S. Ramalingam, S. Sebastian, S. Xavier, S. Periandy, J.C. Daniel, M.M. Julie, DFT, spectroscopic, DSC/TGA, electronic, biological and molecular docking investigation of 2,5-thiophenedicarboxylic acid: a promising anticancer agent, J. Mol. Struct. 1200 (2020) 127099.
[40] J.D. Deephlin Tarika, X.D. Divya Dexlin, S. Madhankumar, D.D. Jayanthi, T.J. Beaula, Tuning the computational evaluation of spectroscopic, ELF, LOL, NCI analysis and molecular docking of novel anti COVID-19 molecule 4-dimethylamino pyridinium 3, 5-dichlorosalicylate, Spectrochim. Acta Part A 259 (2021) 119907.
[41] R. Bastida, A. de Blas, P. Castro, D.E. Fenton, A. Macias, R. Rial, A. Rodriguez, T. Rodriguez-Blas, Complexes of lanthanide (III) ions with macrocyclic ligands containing pyridine head units, J. Chem. Soc. Dalton Trans. 8 (1996) 1493–1497.
[42] N.T. Pour, A. Khalighi, M. Yousefi, V. Amani, One-dimensional barium coordination polymer with 2, 2'-bipyridine-5, 5'-dicarboxylate ligand: synthesis, spectroscopic characterization, thermal analyses, and crystal structure, Synth. React. Inorg. Met. Org. Nano Metal Chem. 45 (2015) 1427–1433.
[43] N. Chetry, T.G. Devi, T. Karloa, Synthesis and characterization of metal complex amino acid using spectroscopic methods and theoretical calculation, J. Mol. Struct. 1250 (2022) 131670.
[44] H.E. Hashema, A. Nathb, A. Kumer, Synthesis, molecular docking, molecular dynamic, quantum calculation, and antibacterial activity of new Schiff base-metal complexes, J. Mol. Struct. 1250 (2022) 131915.
[45] J.A. Obaleyea, M. Lawal, R.N. Jadeja, V.K. Gupta, G.G. Nnabuike, M. Ol. Bamigboye, H. Roy, O.K. Yusuff, A.T. Raji, Cu(II) complex based on lemofloxacin and N,N-donor ligand: synthesis, crystal structure, DFT calculations, and *in vitro* antimicrobial evaluation, J. Mol. Struct. 1249 (2022) 131542.
[46] P.E.M. Amaral, M. Zeller, M. Nozari, A.W. Addiso, 1,3Bis(NMethyl benzimidazol2′yl)2Phenylpropanedichloridocopper(II), J. Chem. Crystallog. (2022), doi:10.1007/s10870-021-00914-0.
[47] R. Konakanchi, P. Jyothi, L.R. Kotha, Investigation of structures, FTIR, FT-Raman, *in vivo* anti-inflammatory, molecular docking and molecular characteristics of 2-amino-3-pyridine carboxaldehyde and its copper(II) complex using experimental and theoretical approach, Polycycl. Aromat. Compd. 42 (1) (2022) 226–248.
[48] M.A. El-ghamry, M. Shebl, A.A. Saleh, S.M.E. Khalil, A.A.M. Ali, M. Dawy, Spectroscopic characterization of Cu(II), Ni(II), Co(II) complexes, and nano copper complex bearing a new S, O, N-donor chelating ligand. 3D modeling studies, antimicrobial, antitumor, and catalytic activities, J. Mol. Struct. 1249 (2022) 131587.
[49] J. Fang, J. Li, Quantum chemistry study on the relationship between molecular structure and corrosion inhibition efficiency of amides, J. Mol. Struct. 593 (2002) 179–185.
[50] T.A. Yousef, G.M. Abu El–Reash, R.M. El Morshedy, Quantum chemical calculations, experimental investigations and DNA studies on (E)-2-((3- hydroxynaphthalen-2-yl)methylene)-N-(pyridin-2-yl)hydrazinecarbothioamide and its Mn(II), Ni(II), Cu(II), Zn(II) and Cd(II) complexes, Polyhedron 45 (2012) 71–85.
[51] E.M.A. Valle, V.G. Maltarollo, M.O. Almeida, K.M. Honorio, M.C. dos Santos, G. Cerchiaro, Time dependent-density functional theory (TD-DFT) and experimental studies of UVeVisible spectra and cyclic voltammetry for Cu(II) complex with Et2DTC, J. Mol. Struct. 1157 (2018) 463–468.
[52] T.I K.Ohno, C. Yokota, Y. Katsumoto, Matrix-isolation infrared spectra of 2-, 3- and 4-pyridinecarboxaldehyde before and after UV irradiation, J. Mol. Struct. 825 (2006) 143–150.
[53] S. Dekar, K. Ouari, S. Bendia, D. Hannachi, J. Weiss, J. Organomet. Chem. 866 (2018) 165–176.
[54] M. Tahenti, S. Gatfaoui, N. Issaoui, T. Roisnel, H. Marouani, A tetrachlorocobaltate(II) salt with 2-amino-5-picolinium: synthesis, theoretical and experimental characterization, J. Mol. Struct. 1207 (2020) 127781.
[55] C. Daghar, N. Issaoui, T. Roisnel, V. Dorcet, H. Marouani, Empirical and computational studies on newly synthesis cyclohexylammonium perchlorate, J. Mol. Struct. 1230 (2021) 129820.
[56] S. Jenkins, I. Morrison, The chemical character of the intermolecular bonds of sevenphases of ice as revealed by ab initio calculation of electron densities, Chem. Phys. Lett. 317 (2000) 97–102.
[57] E. Espinosa, I. Alkorta, J. Elguero, E. Molins, From weak to strong interactions: a comprehensive analysis of the topological and energetic properties of the electron density distribution involving X–H F–Y systems, J. Chem. Phys. 117 (2002) 5529–5542.
[58] S. Dinda, A.G. Samuelson, The nature of bond critical points in dinuclear copper(I) complexes, Chem. Eur. J. 18 (2012) 3032–3042.
[59] K.M. Chandini, F.H. Al-Ostoot, E.E. Shehata, N.Y. Elamine, H. Ferjani, M.A. Sridhar, N.K. Lokanath, Synthesis, crystal structure, Hirshfeld surface analysis, DFT calculations, 3D energy frameworks studies of Schiff base derivative 2,2-((1Z,1Z)-(1,2-phenylene bis(azanylylidene)) bis(methanylylidene)) diphenol, J. Mol. Struct. 1244 (2021) 130910.
[60] D. Milenkovic, E. Avdovic, D. Dimic, S. Sudha, D. Ramarajan, Z. Milanovic, S. Trifunovic, Z.S. Markovic, Vibrational and Hirshfeld surface analyses, quantum chemical calculations, and molecular docking studies of coumarin derivative 3- (1-m-toluidinoethylidene)-chromane-2,4-dione and its corresponding palladium(II) complex, J. Mol. Struct. 1209 (2020) 127935.
[61] A. Kerflani, K. Si Larbi, A. Rabahi, A. Bouchoucha, S. Zaater, S. Terrachet-Bouaziz, Novel palladium (II) complexes with iminocoumarin ligands: synthesis, characterisation, electrochemical behaviour, DFT calculations and biological activities, ADMET study and molecular docking, Inorg. Chim. Acta 529 (2022) 120659.
[62] C. Kucuk, S. Yurdakul, B. Erdem, Experimental and theoretical Fourier transform infrared and Raman spectroscopy, density functional theory, antibacterial activity and molecular docking studies on 1(4methoxyphenyl)1Himidazole, Chem. Pap. (2022).
[63] C. Tabares-Mendoza, P. Guadarrama, Predicting the catalytic efficiency by quantum-chemical descriptors: theoretical study of pincer metallic complexes involved in the catalytic Heck reaction, J. Organomet. Chem. 691 (2006) 2978–2986.
[64] R. Parthasarathi, V. Subramanian, D.R. Roy, P.K. Chattaraj, Electrophilicity index as a possible descriptor of biological activity, Bioorg. Med. Chem. 12 (21) (2004) 5566–15543.
[65] F. Basha, F.L. Ali Khana, S. Muthu, M. Raja, Elaborated molecular structure, molecular docking and vibrational spectroscopic investigation of N-((4-aminophenyl)sulfonyl)benzamide with density functional theory, Chem. Data Collect. 31 (2021) 100609.
[66] S. Pangajavalli, R. Ranjith Kumar, S. Ramaswamy, Structural, Hirshfeld, spectroscopic, quantum chemical and molecular docking studies of N'-(4-(4-Chlorophenyl)-1,3-dicyano-5,6,7,8,9,10- hexahydrobenzo[8]annulen 2-yl) N,N-dimethylformimidamide as CCR2 inhibitors, J. Mol. Struct. 1239 (2021) 130503.
[67] A. Fatima, G. Khanum, S. Savita, K.M. Pooja, I. Verma, N. Siddiqui, S. Javed, Quantum computational, spectroscopic, Hirshfeld surface, electronic state and molecular docking studies on sulfanilic acid: an anti-bacterial drug, J. Mol. Liq. (2022), doi:10.1016/j.molliq.2021.117150.
[68] N. Tiwari, A. Pandey, A. Kumar, A. Mishra, Computational models reveal the potential of polycyclic aromatic hydrocarbons to inhibit aromatase, an important enzyme of the steroid biosynthesis pathway, Comput. Toxicol. 19 (2021) 100176.
[69] B. Sun, C. Liu, D. Che, H. Liu, S. Guo, Density functional theory–based investigation of CaO/char catalyzing the transformation of NH3 to N2, J. Anal. Appl. Pyrol. 156 (2021) 105124.
[70] S.K. Patel, R.N. Patel, A.K. Patel, N. Patel, I. Coloma, M. Cortijo, S. Herrero, D. Choquesillo-Lazarte, Synthesis, single crystal structures, DFT and *in vitro* anti oxidant superoxide dismutase studies of copper(II) complexes derived from the di-(2-picolyl) amine and co-ligands: Promising antioxidants, Polyhedron 212 (2022) 115609.
[71] X. Zhao, Z. Yu, T. Ding, Quorum-sensing regulation of antimicrobial resistance in bacteria, Microorganisms 8 (2020) 425, doi:10.3390/microorganisms8030425.
[72] W. Chu, D.A. Vattem Maitin, V. Barnes, M.B. McLean, Bioassays of quorum sensing compounds using agrobacterium tumefaciens and chromobacterium violaceum, Methods Mol. Biol. 692 (2011) 3–19.
[73] T.J. Beaula, P. Muthuraja, M. Sethuram, M. Dhandapani, V.K. Rastogi, V.B. Jothy, Biological and spectral studies of O-tolyl biguanide: experimental and theoretical approach, J. Mol. Struct. 1128 (2017) 290–299.
[74] N. Balakrishnan, J. Haribabu, R. Eshaghi Malekshah, S. Swaminathan, C. Balachandran, N. Bhuvanesh, S. Aoki, R. Karvembu, Effect of N-benzyl group in indole scaffold of thiosemicarbazones on the biological activity of their Pd(II) complexes: DFT, biomolecular interactions, in silico docking, ADME and cytotoxicity studies, Inorg. Chim. Acta 534 (2022) 120805.
[75] A. Üngördü, N. Tezer, Effect on frontier molecular orbitals of substituents in 5-position of uracil base pairs in vacuum and water, J. Theor. Comput. Chem. 16 (07) (2017) 1750066.
[76] X.D. Divya Dexlin, J.D. Deephlin Tarika, M. Sethuram, T. Joselin Beaula, Synthesis, vibrational depictions, IRI interpretations and docking research on coordination metal complex Diaqua aspartato zinc (II) monohydrate using DFT approach, J. Mol. Liq. 351 (2022) 118687.
[77] R.A. Laskoswki, M.W. MacArthur, Moss DS PROCHECK: a program to check the stereochemical quality of protein structures, J. Appl. Crystallogr. 26 (1993) 283–291.